

# Quantum Diffusion and Localization in Disordered Electronic Systems

P. R. Wells Jr.,\* J. d'Albuquerque e Castro,<sup>†</sup> and S. L. A. de Queiroz<sup>‡</sup>

*Instituto de Física, Universidade Federal do Rio de Janeiro,*

*Caixa Postal 68528, 21941-972 Rio de Janeiro RJ, Brazil*

(Dated: February 9, 2022)

The diffusion of electronic wave packets in one-dimensional systems with on-site, binary disorder is numerically investigated within the framework of a single-band tight-binding model. Fractal properties are incorporated by assuming that the distribution of distances  $\ell$  between consecutive impurities obeys a power law,  $P(\ell) \sim \ell^{-\alpha}$ . For suitable ranges of  $\alpha$ , one finds system-wide anomalous diffusion. Asymmetric diffusion effects are introduced through the application of an external electric field, leading to results similar to those observed in the case of photogenerated electron-hole plasmas in tilted InP/InGaAs/InP quantum wells.

PACS numbers: 72.15.Rn, 71.23.-k, 71.23.An

## I. INTRODUCTION

The work reported in this paper is motivated by the experimental observation of asymmetric diffusion of electron-hole plasmas in semiconductor quantum wells<sup>1,2,3</sup>, as well as by attempts at a theoretical explanation of such results, on the basis of models for fractal diffusion<sup>1,4</sup>. In Ref. 1, electron-hole plasmas were photogenerated in intrinsic InP/InGaAs/InP single quantum wells, and their diffusion was observed through measurements of photoluminescence intensity profiles. Two types of heterostructures were examined: the first was grown in a direction normal to the [001] crystallographic axis, and the second was grown in a direction tilted by 2° relative to that of the first, toward the [111] axis. The experimental results were as follows: in the former structure the plasma undergoes Gaussian (symmetric) diffusion, while in the latter the diffusion is asymmetric. The authors of Ref. 1 showed that diffusion data for the tilted heterostructure can be fitted by an asymmetric Lévy distribution, previously obtained<sup>4</sup> as a solution to a (one-dimensional) generalized Fokker-Planck equation with distinct right- and left- diffusion coefficients, and fractional derivatives. Furthermore, it was argued that the fractional character of the diffusion is connected to fractal properties of the medium, namely a power-law roughness distribution of the interfaces that delimit the quantum wells. Further photoluminescence studies suggest that the carrier diffusion properties are indeed very sensitive both to interface roughness, and to the presence of finite-width terraces<sup>2</sup>. By varying both optical excitation intensities and temperature, a more detailed picture was found for the anomalous diffusion phenomena taking place, including the likely existence of Auger recombination, which in its turn might be induced by fractal interface morphology<sup>3</sup>.

The relationship between fractional diffusion and the absence of a characteristic length scale (the latter being a basic property of fractals) is well-established, and has been extensively investigated<sup>5,6,7</sup>.

Here we study a model system along the lines of Anderson's picture<sup>8,9,10,11</sup> for electron diffusion in disordered media. Alternatively to the theoretical approach

adopted in Refs. 1,4, whose starting point was a generalized Fokker-Planck equation for (classical) particles, we write a tight-binding Hamiltonian for a (quantum) particle, which evolves according to the rules of quantum mechanics. The fractal features are incorporated by a specific spatial distribution of on-site disorder, to be described below.

Bearing in mind that the electron-hole pairs undergoing anomalous diffusion in the experimental systems are essentially quantum-mechanical objects, our treatment is expected to reflect the basic wave-like properties of such entities. The link between the quantum properties underlying localization, and those classical features brought to fore in classical approaches to diffusion is not well understood, although it has been discussed in the recent past (see, e.g., Ref. 12).

Our main concern is to provide an independent check of whether the connection between fractal properties of a disordered medium, and the behavior of particles diffusing in it, which has been proposed in the classical context, is robust enough to survive the translation to a quantum-mechanical picture. Therefore, we shall not aim at making specific comparisons of our results to the experiments described in Refs. 1,2,3.

In Subsection II A, we introduce the tight-binding hamiltonian and the respective disorder distributions to be investigated, along with a brief description of our calculational procedures. In Subsection II B results are given for the time evolution of the width of wavefunction packets against time, as well as for the corresponding instantaneous profiles. Subsection II C deals with the introduction of an external bias, in order to investigate the effects of anisotropy. Finally, in Sec. III, concluding remarks are made.

## II. MODEL SYSTEM AND RESULTS

### A. Model

In order to simplify the calculational framework, we restrict our investigation to one-dimensional systems. We

consider the one-electron, tight-binding hamiltonian for a single-orbital linear chain with nearest neighbor hopping,

$$H = \sum_n |n\rangle \epsilon_n \langle n| - \gamma \sum_{n,m} |n\rangle \langle m|, \quad (1)$$

where  $|n\rangle$  is an orbital with self-energy  $\epsilon_n$ ,  $m = n \pm 1$ , and  $\gamma$  is the hopping energy, assumed to be constant and positive.

We study binary models of disordered alloys, in which two different orbitals  $A$  (host atoms) and  $B$  (substitutional impurities) coexist, with respective self-energies  $\epsilon_A$  and  $\epsilon_B$ , and overall concentrations  $1 - p_0$  and  $p_0$ . The relevant energy in the present context is  $\epsilon \equiv \epsilon_B - \epsilon_A$ , which measures the impurity-host mismatch.

If the impurity locations are uncorrelated, (a case to be denoted as the *random binary model*, or random for short) the distances  $\ell$  between any two consecutive impurities have an exponential distribution, i.e.,

$$P(\ell) = \frac{p_0}{1 - p_0} (1 - p_0)^\ell \sim \exp(-\lambda\ell) \quad (\ell = 1, 2, \dots), \quad (2)$$

where  $\lambda = \lambda(p_0) = -\ln(1 - p_0)$  is the inverse decay length (in lattice parameter units) that sets a scale for the typical  $B - B$  distance, i.e., a cutoff dictating the largest allowable distances. Note that the *average* impurity-impurity distance is  $p_0^{-1}$ , which approaches  $\lambda^{-1}$  only in the low-concentration limit  $p_0 \ll 1$  where continuum and discrete-lattice descriptions become equivalent. For the random model, host-impurity ( $A - B$ ) duality means that our investigation can be restricted to  $0 \leq p_0 \leq 1/2$ .

We introduce fractal features by assuming the distribution of  $\ell$  to decay with a power law:

$$P(\ell) \sim \ell^{-\alpha}, \quad (3)$$

where  $\alpha$  is a characteristic exponent.

Distributions similar to Eq. (3) have been extensively studied in the literature of fractal-based point processes<sup>13,14,15</sup>; in that context, they refer to the probabilities of occurrence of interevent (time) separations. In such cases, most of the interest focuses on the characteristics of the associated power spectrum, which turns out to exhibit  $1/f^\alpha$  noise properties. Here, by contrast, the fractal features of the real-space impurity distribution are of interest only inasmuch as they are the background against which we simulate the quantum-mechanical evolution of electronic wavepackets.

The distribution given by Eq. (3) is normalizable only for  $\alpha > 1$ ; its mean is finite only for  $\alpha > 2$ , and its variance is finite only for  $\alpha > 3$ . Nevertheless, as discussed at length in Subsec. II B, it is a physically sensible choice to adopt a system-wide normalization which enables one to consider  $1 < \alpha \leq 2$ , for (large but finite) fractal systems. In this *fractal binary model*, or fractal, for short,  $\ell$  lacks a typical scale. Here, all distances are allowed, on account of the slowly-decaying distribution tail. Thus we expect the resulting system to exhibit fractal properties, provided that it is large enough. The correlation

between impurity positions, implied by Eq. (3), destroys strict  $A - B$  duality.

Comparison between overall concentrations in the two cases proceeds by matching the respective average distances between impurities, which are  $p_0^{-1}$  for the former model [ as remarked in connection with Eq. (2) ] and  $\zeta(\alpha - 1)/\zeta(\alpha)$  for the latter, where  $\zeta(\alpha) = \sum_{n=1}^{\infty} n^{-\alpha}$  is Riemann's zeta function. For example,  $p_0 = 0.4 \leftrightarrow \alpha \approx 2.34$ . Clearly, in the thermodynamic limit any  $\alpha \leq 2$  corresponds to vanishing  $B$  concentrations in the fractal. However, as pointed out above, for large but finite systems one can still get nontrivial results for  $\alpha \leq 2$ , once suitable normalization considerations are taken into account [ see Fig. 3 below, for a full illustration of the  $p_0 - \alpha$  correspondence, both in the thermodynamic limit and for finite systems; see also Eq. (6) ].

We study the dynamics of wave packets<sup>16,17</sup> in random and fractal linear chains. The time evolution of the amplitudes  $\psi_n(t) = \langle n | \psi(t) \rangle$  is determined by the Schrödinger equation:

$$i\dot{\psi}_n = \varepsilon_n \psi_n - \psi_{n-1} - \psi_{n+1}, \quad (4)$$

where  $\varepsilon_n = \epsilon_n/\gamma$  is a dimensionless parameter, and time is given in units of  $\hbar/\gamma$ .

We start with Gaussian wave packets:

$$\psi_n(0) = C \exp \left[ \frac{-(n - n_0)^2}{2\sigma_0^2} \right], \quad (5)$$

where  $n_0$  denotes the initial position of the centroid, and  $\sigma_0$  the initial width, and  $C$  is a normalization constant.

Configurational averages are taken in all the calculations presented in this work.

## B. Variances and wave fronts

We analyze and compare the properties of the two kinds of systems just defined.

We have numerically determined the time evolution of the (ensemble-) averaged wave-packets in one-dimensional systems of sizes  $L = 10000$ , with free ends. The number of realizations incorporated in the ensemble averages is  $M = 1000$  or, in some cases, larger.

The calculational method is based on numerical integration of Eq. (4) with initial condition given by Eq. (5), via a fifth-order Runge-Kutta code. We compared results for fixed realizations of disorder, obtained with time steps of 0.1 and 0.01, and checked that they are indistinguishable for all practical purposes. Thus, we set the former value in all calculations described here.

The integration is taken up to times not longer than enough for the packet to reach the chain's ends, in order to avoid reflection effects. The actual hopping-rate of an electron in a pure system modeled by Eq. (4) is one atom per time unit. Considering that diffusion on a disordered chain is hampered by impurities, in order to be safe we set the upper time limit as  $L/2$ , for a packet initially

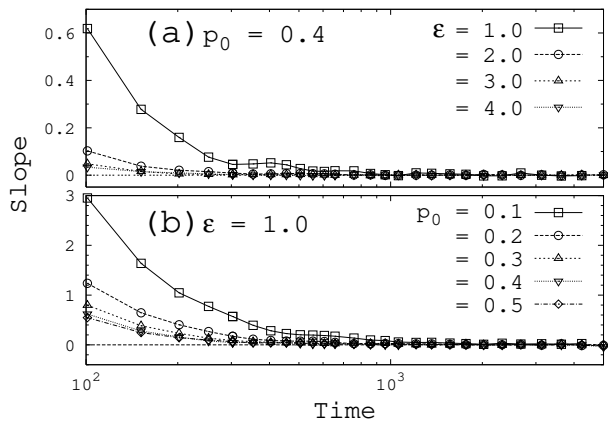


Figure 1: Plots of slopes (time derivatives)  $d\langle(\Delta x)^2\rangle/dt$  of variances of particle probability distribution against time in the random system. In (a)  $\varepsilon = 1.0$  for several  $p_0$ , while in (b),  $p_0 = 0.4$  for several  $\varepsilon$ .  $L = 10\,000$  and  $M = 10^3$  samples each.

spread over a few sites around the center of an  $L$ -atom chain. We have used  $\sigma_0 = 5.0$ , that is, the initial packets are rather localized.

As usual, we study diffusional behavior through investigation of the time evolution of the ensemble-averaged second moment (variance) of the particle probability distribution,  $\langle(\Delta x)^2\rangle$ . Power-law dependencies,  $\langle(\Delta x)^2\rangle \sim t^{2\beta}$ , with  $\beta = 0, 1/2$ , and  $1$  characterize localized, diffusive, and “ballistic” regimes respectively (the latter to be interpreted here in the sense that, even though there is no center-of-mass motion in the absence of an external bias, the packet width varies linearly in time if each of its Fourier components travels unhindered).

Initially we consider the random model, so as to provide a benchmark against which to compare results for the fractal case.

By scanning the values of  $\varepsilon \equiv \epsilon/\gamma$  for the dimensionless impurity-host self-energy mismatch, as well as those of  $p_0$ , along suitable intervals, one finds the same overall picture, namely apparent ballistic behavior at first, followed by a continuous, smooth crossover towards localization, i.e. the variances  $\langle(\Delta x)^2\rangle$  eventually approach saturation. To illustrate this, in Figure 1 we show the evolution of the slopes  $d\langle(\Delta x)^2\rangle/dt$  against time, in the random system. One can see that saturation behavior (zero slope) always obtains, albeit at rates which depend on  $\varepsilon$  and  $p_0$ .

We have found no simple scaling picture, from which a data collapse plot could be derived. Even for fixed  $\varepsilon$ , where for each  $p_0$  one has the characteristic inter-impurity distance  $\lambda^{-1}(p_0)$ , this quantity does not translate directly on to a scaling length. In this case, the saturation value of  $\langle(\Delta x)^2\rangle$  varies approximately as  $p_0^{-1.35}$  (for  $p_0 \leq 0.5$ ).

We now turn to the fractal model, for which representative results are shown in Fig. 2. These are for samples whose distributions  $P(\ell)$  are normalized with respect to

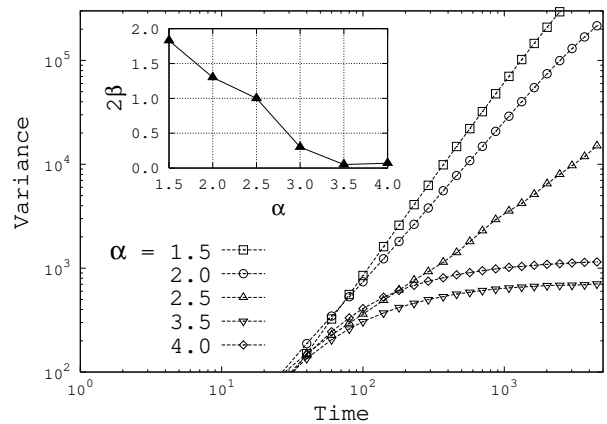


Figure 2: Double-logarithmic plots of variance of particle probability distribution against time in the fractal system, for  $\varepsilon = 1.0$  and several  $\alpha$  (see text for explanation of  $\alpha \leq 2$  data).  $L = 10\,000$  and  $M = 5 \times 10^3$  samples each [except  $\alpha = 1.5$  for which  $M = 10^3$ ]. Inset: asymptotic characteristic exponent  $2\beta$  as a function of  $\alpha$ , for data on the main diagram (see text).

the actual system size  $L$ , i.e.,

$$P(\ell) = \frac{\ell^{-\alpha}}{\zeta_L(\alpha)}, \quad \zeta_L(\alpha) \equiv \sum_{n=1}^L \frac{1}{n^\alpha}. \quad (6)$$

Such a system-wide normalization is indeed consistent with the inclusion-exclusion principle. This can be seen by recalling that, starting from a  $B$  atom at  $x = 0$  and following along the chain, the statement that, e.g., the first  $B$  atom occurs at  $x = \ell$  encompasses all (mutually exclusive)  $2^{L-\ell}$  possible arrangements of  $A$ 's and  $B$ 's, for  $x > \ell$ , and with *only*  $A$ 's for  $1 \leq x \leq \ell - 1$ . With the above normalization, even for  $\alpha \leq 2$  one has, on average, a non-vanishing (though in such case rather small) impurity concentration. This is illustrated in Fig. 3.

The larger the system, the individual probabilities for some given distance  $\ell$  become comparatively smaller, while the occurrence of larger distances becomes possible, although with low probability. We find that for larger systems, the fractal environment makes it easier for the packet to diffuse than the random one, for the same (effective) concentration of impurities. Of course, here one is only considering diffusion along distances of the order of the system's length,  $L$ . The crucial difference, relative to the random model, is that since there is no intrinsic length scale in the fractal system, the single length introduced by the normalization in Eq. (6) coincides with the system size. Thus, although the diffusive behavior observed here must always be regarded as an apparent regime, it may extend to rather long distances.

The occurrence of large impurity-impurity distances in this system may produce individual realizations of disorder, comprising regions that are effectively pure. The result is that the eigenstates in the system may be ex-

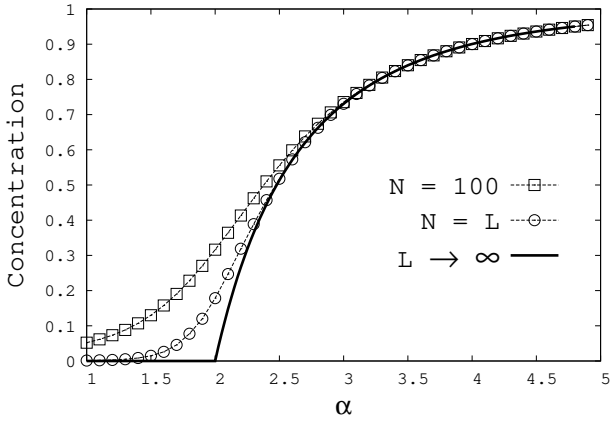


Figure 3: Effective average concentration  $p_0$  of impurity sites in the fractal model, against  $\alpha$ .  $L \rightarrow \infty$  refers to Eq. (6) in such limit, while points are for  $L = 10\,000$ , with normalization by  $N$  [ $N = L$  is system-wide normalization as in Eq. (6)]; see text.

tended, or semi-extended. Averaging over many realizations would produce an ensemble of wave packets composed of localized and extended states, even though on average the system has a finite concentration of impurities. Least-squares fits of  $10^2 < t < 5 \times 10^3$  data of Figure 2 to a single power-law form produce an exponent  $2\beta = 1.82(1)$ ,  $1.30(1)$ , and  $1.04(1)$  respectively for  $\alpha = 1.5$ ,  $2.0$ , and  $2.5$ . Thus one finds an effective anomalous diffusion regime, which has no counterpart in the random disorder model.

On the other hand, the  $\alpha = 3.5$  results, for example, show that even in the fractal model, one can have disorder so strong that localization (within the system's limits) is statistically the only possible outcome. For this case, the corresponding effective impurity concentration, as defined above, is  $\approx 0.84$ , which (for the random model) would be equivalent to  $p_0 = 0.16$ , by using the  $p_0 \leftrightarrow 1 - p_0$  duality valid for the latter type of disorder. One can infer from Fig. 1 (b) that the behavior of the  $p_0 = 0.16$  random system is indeed similar to that of the  $\alpha = 3.5$  fractal case, namely localization setting in for  $t \approx 10^3$  [we have also checked that the actual saturation value of  $\langle(\Delta x)^2\rangle$ , which is  $\approx 6 \times 10^2$  for  $\alpha = 3.5$  (fractal), falls between the respective ones for  $p_0 = 0.1$  and  $0.2$  (random)].

As regards  $\alpha = 4.0$  data, for which one has the equivalent  $p_0 = 0.90$  from Fig. 3, comparison is to be made to the  $p_0 = 0.10$  curve of Fig. 1 (b). Again, the agreement is very good, as far as general trends are concerned: increasing  $\alpha$  in this range turns out to produce a longer localization length.

The reason why the fractal model behaves similarly to the random one for large  $\alpha$ , while it certainly does not do so for  $\alpha \leq 2.5$ , is as follows. From Eqs. (3) and (6), one can work out that the probability distribution for

distances between consecutive  $A$  atoms is

$$P_A(\ell) \sim \exp[a(\alpha)\ell], \quad a(\alpha) = \ln P(1), \quad (7)$$

where  $P(1) = \zeta_L^{-1}(\alpha)$  is the probability for unit distance between  $B$  (impurity) atoms. For  $\alpha \leq 2.5$  (corresponding to  $p_0 \leq 0.5$ ), the  $B$  atoms are in the minority, so they indeed play the role of impurities in an otherwise pure  $A$  system. As seen above, the fractal properties associated to the power-law  $B - B$  distance distribution, Eq. (3), give rise to the consequent diffusion-like behavior. At larger  $\alpha$  ( $p_0 > 0.5$ ), the  $A$  atoms are now in the minority. Physically, the traveling electrons are only sensitive to the existence of two distinct values of on-site energies, thus the effective "impurity" label will be assigned in practice to the species which occurs less frequently (in this case,  $A$  atoms, whose distance distribution, Eq. (7), is qualitatively the same as in the random model, thus bringing about localization). The characteristic length,  $[\ln \zeta_L(\alpha)]^{-1}$ , increases with increasing  $\alpha$ , thus explaining the trend mentioned above.

In practice, one would expect the region  $0.4 \lesssim p_0 \lesssim 0.6$ , i.e.,  $2.35 \lesssim \alpha \lesssim 2.65$ , to behave as a crossover region. This is because, for the finite systems under study, one needs a clear majority of one species over the other to be statistically established while still within distances shorter than system size.

Further evidence that effective diffusion-like behavior is linked to the absence of a typical scale in fractal systems can be derived as follows. If, instead of normalizing  $P(\ell)$  by system size  $L$  as in Eq. (6), we take a fixed  $N < L$  as the upper limit (see in Fig. 3 how this affects the effective impurity concentration), a length scale equal to  $N$  is introduced, even though the variation of  $P(\ell)$  against  $\ell$  is still described by a power law. Results for  $N = 100$ , and assorted values of  $\alpha$  are shown in Fig. 4. Note that while the localization length decreases with increasing  $\alpha \leq 2.5$ , the trend is reversed for  $\alpha > 2.5$ . This is similar in nature to the  $p_0 \leftrightarrow 1 - p_0$  duality observed in the random model.

Finally, we examine the actual shapes of particle probability densities. For the localized packets in the random case, extended exponentials,  $|\psi(x)|^2 \sim \exp(-b|x|^\phi)$ , provide reasonably good fits to the region within 20 to 30 sites from the peak, with  $1.5 \lesssim \phi \lesssim 1.8$ . At larger distances, the probability density decay is somewhat slower than that. Fits for  $30 \lesssim x \lesssim 200$  give  $\phi$  in the  $0.2 - 0.6$  range.

On the other hand, for the fractal cases with apparent diffusion, one can get power-law fits extending to two or more decades of distance, as shown in Fig. 5. Of course, the power-law behavior exhibited in the Figure is expected to hold only within the system's finite limits, as is the case for all features of the apparent diffusion regime (recall that our whole study is conducted for times not longer than enough for the wavepacket to reach the chain's ends, in order to avoid reflection effects). Thus, for instance, although data for  $\alpha = 1.5$  (corresponding

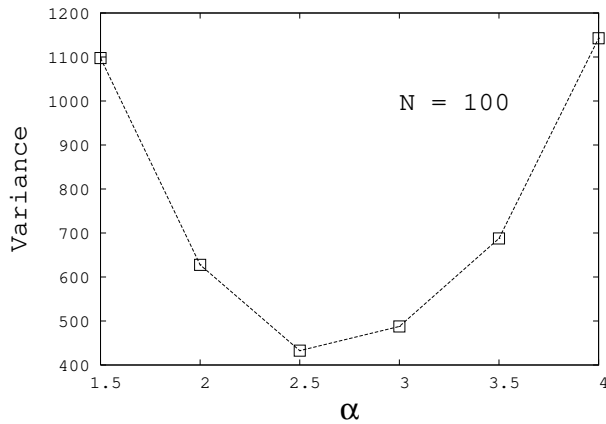


Figure 4: Asymptotic values of variance of particle probability distribution in the fractal system, with  $P(\ell) = 0$  for  $\ell > 100$ , and the corresponding normalization (see text), for  $\varepsilon = 1.0$  and several  $\alpha$ .  $L = 10\,000$  and  $M = 10^3$  samples each.

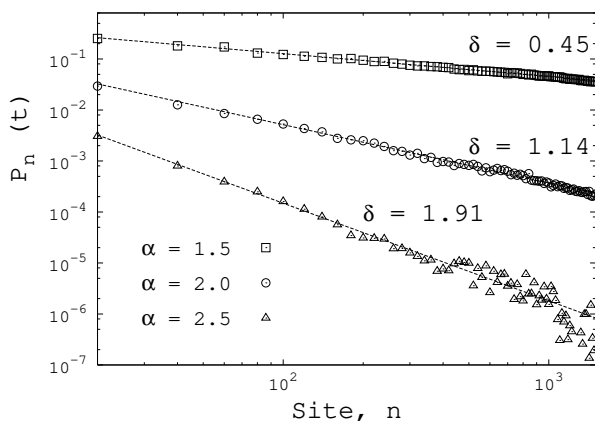


Figure 5: Double-logarithmic plots of particle probability distribution functions against position, at  $t = 5000$ , for assorted values of  $\alpha$  in the (apparent) diffusive regime.  $\varepsilon = 1.0$ ,  $L = 10\,000$ , and  $M = 10^3$  samples. Lines indicate least-squares fits to a power-law form,  $P(x) \sim x^{-\delta}$ . See text for a discussion of suitable normalization considerations.

to power-law decay with  $\delta = 0.45$ ) would be strictly non-normalizable if such behavior extended to arbitrarily long distances, one must keep in mind that (within the present context) the wavepacket amplitude will fall to zero before reaching the chain's ends. Localized packets for fractal disorder, i.e.,  $\alpha \gtrsim 3.0$  (not shown), seem to behave in an intermediate way between power-law and extended exponential decay.

### C. Application of a bias

We search for an effect that, in the present quantum-mechanical formulation, would be the equivalent to distinct values for left- and right- diffusion coefficients in

the Fokker-Planck approach of Refs. 1,4. The simplest source of such anisotropy is an electric field.

The effect of applying a uniform electric field to the system is incorporated by the inclusion of the term

$$H_{bias} = \sum_n |n\rangle e E n \langle n| \quad (8)$$

in the Hamiltonian, where  $e$  is the electronic charge, and  $E$  is the field intensity. The corresponding Schrödinger equation is

$$i \dot{\psi}_n = (\varepsilon_n + f_0 n) \psi_n - \psi_{n-1} - \psi_{n+1}, \quad (9)$$

where  $f_0 = e E / \gamma$  is a dimensionless bias intensity.

On a pure system, application of a bias produces a drift of the entire wave packet, as its centroid moves through the lattice, with diffusion occurring with respect to the center-of-mass reference frame. However, due to the unequal effect of the bias on the various Fourier components of the packet, this diffusion may be asymmetric. Also, one must be aware of Bloch oscillations, which confine the wave packet in a region of space, thus producing oscillating behavior from application of a static electric field<sup>18</sup>.

In order to prevent the effect of Bloch oscillations from distorting the diffusive behavior which is our main concern, here we use  $f_0 = 1.0 \times 10^{-3}$ . Then, elementary considerations show that for a packet starting at the center of a chain with  $L = 10\,000$ , speed reversal will only set in at  $t \lesssim 4 \times 10^3$ , giving one a rather broad window of observation.

In a disordered system, the application of a bias gives rise to dynamical localization. This is related to Bloch oscillations. The difference is that a part of the packet diffuses away and performs oscillations, while the other part remains localized close to the origin. Such asymmetric diffusion behavior may thus be viewed as the coexistence of two distinct regimes.

The results in Fig. 6 show that the diffusing portion of the averaged wave packet behaves as if the system were pure; its centroid coincides with that of a corresponding wave packet in a pure system. One can see that it is only for the fractal case with apparent diffusion ( $\alpha = 2.5$ ) that a significant portion of the particle probability distribution is pure-system-like. As remarked above, for such values of  $\alpha$  one has coexistence between individual disorder realizations with effectively delocalized eigenstates, and others in which localization occurs. The relative height of the corresponding peaks in Fig. 6 shows that the latter are much more frequent than the former.

### III. DISCUSSION AND CONCLUSIONS

We have introduced a model system for the incorporation of on-site fractal disorder in the one-electron diffusion problem. As remarked above, the distribution of

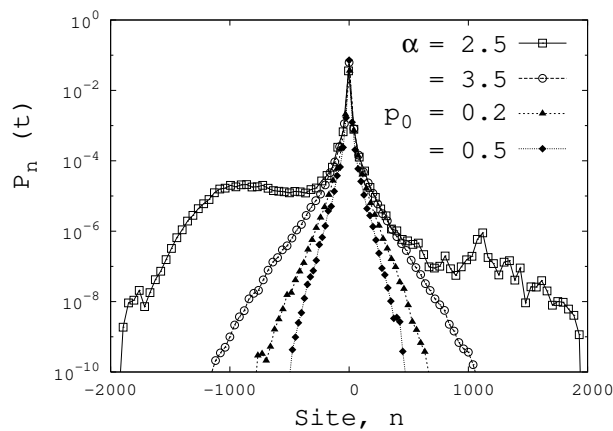


Figure 6: Particle probability distribution against position, for  $t = 1000$ ,  $f_0 = 1.0 \times 10^{-3}$  for  $\varepsilon = 1.0$ .  $L = 10000$  and  $M = 10^3$  samples each [except  $\alpha = 2.5$  for which  $M = 5 \times 10^3$ ]. Open symbols: fractal systems; full symbols: random systems.

impurity-impurity distances given in Eq. (3) implies that disorder is in fact correlated. It is well known that features such as long-range hopping<sup>19,20</sup> and/or correlated disorder<sup>21,22,23,24,25</sup> may have strong effects (including the occurrence of a metal-insulator transition even in one-

dimensional systems), an observation which is confirmed here by the comparison of fractally-disordered and uncorrelated random electronic systems.

As regards comparison with experimental results, the wavefront profiles depicted in Fig. 6 show a connection between anomalous diffusion of tight-binding electrons and fractal properties of the underlying medium. Furthermore, we have seen that, in the present model, asymmetric profiles arise from coexistence of ballistic and localized states upon application of an external bias. Such coexistence results from the fact that a subset of ensemble realizations of the (scale-free) disorder are, in fact, almost pure. Whether the same explanation holds for the experimentally-observed profiles is not certain at the moment, though one might conceivably propose ways to test it on available samples.

### Acknowledgments

We thank A. S. Chaves and F. A. B. F. de Moura for interesting conversations. This research was partially supported by the Brazilian agencies CAPES, CNPq, FAPERJ (Grant No. E26-100.604/2007), and Instituto do Milênio de Nanotecnologia-MCT.

\* Electronic address: wells@if.ufrj.br

† Electronic address: jcastro@if.ufrj.br

‡ Electronic address: sldq@if.ufrj.br

<sup>1</sup> A. F. G. Monte, S. W. da Silva, J. M. R. Cruz, P. C. Morais, A. S. Chaves, and H. M. Cox, Phys. Lett. A **268**, 430 (2000).

<sup>2</sup> A. F. G. Monte, S. W. da Silva, J. M. R. Cruz, P. C. Morais, and A. S. Chaves, Appl. Phys. Lett. **81**, 2460 (2002).

<sup>3</sup> J. B. Borges, S. W. da Silva, P. C. Morais, and A. F. G. Monte, Appl. Phys. Lett. **89**, 142103 (2006).

<sup>4</sup> A. S. Chaves, Phys. Lett. A **239**, 13 (1998).

<sup>5</sup> R. Metzler and J. Klafter, Phys. Rep. **339**, 1 (2000).

<sup>6</sup> G. Zaslavsky, Phys. Rep. **371**, 461 (2002).

<sup>7</sup> I. Calvo, R. Sánchez, B. A. Carreras, and B. Ph. van Milligen, Phys. Rev. Lett. **99**, 230603 (2007).

<sup>8</sup> P. W. Anderson, Phys. Rev. **109**, 1492 (1958).

<sup>9</sup> E. Abrahams, P. W. Anderson, D. C. Licciardello, and T. V. Ramakrishnan, Phys. Rev. Lett. **42**, 673 (1979).

<sup>10</sup> B. Kramer, G. Bergmann, and Y. Bruynseraede, *Localization, Interaction and Transport Phenomena*, Springer Series in Solid State Sciences Vol. 61 (Springer, Berlin, 1985).

<sup>11</sup> B. Kramer and A. MacKinnon, Rep. Prog. Phys. **56**, 1469 (1993).

<sup>12</sup> A. M. Garcia-Garcia, Phys. Rev. E **69**, 066216 (2004).

<sup>13</sup> S. B. Lowen and M. C. Teich, Phys. Rev. B **46**, 1816 (1992).

<sup>14</sup> S. B. Lowen and M. C. Teich, Phys. Rev. E **47**, 992 (1993).

<sup>15</sup> S. B. Lowen and M. C. Teich, *Fractal-Based Point Processes* (Wiley, 2005).

<sup>16</sup> H. Yamada and M. Goda, Phys. Lett. A **194**, 279 (1994).

<sup>17</sup> J. Zhong, R. B. Diener, D. A. Steck, W. H. Oskay, M. G. Raizen, E. W. Plummer, Z. Zhang, and Q. Niu, Phys. Rev. Lett. **86**, 2485 (2001).

<sup>18</sup> J. Feldmann, K. Leo, J. Shah, D. A. B. Miller, J. E. Cunningham, T. Meier, G. von Plessen, A. Schulze, P. Thomas, and S. Schmitt-Rink, Phys. Rev. B **46**, 7252(R) (1992); K. Leo, Semicond. Sci. Technol. **13**, 249 (1998).

<sup>19</sup> E. N. Economou, C. M. Soukoulis, and M. H. Cohen, Phys. Rev. B **37**, 4399 (1988).

<sup>20</sup> D. B. Balagurov, V. A. Malyshev, and F. D. Adame, Phys. Rev. B **69**, 104204 (2004).

<sup>21</sup> D. H. Dunlap, H-L. Wu, and P. W. Phillips, Phys. Rev. Lett. **65**, 88 (1990).

<sup>22</sup> P. W. Phillips and H-L. Wu, Science **252**, 1805 (1991).

<sup>23</sup> C. M. Soukoulis, M. J. Velgakis, and E. N. Economou, Phys. Rev. B **50**, 5110 (1994).

<sup>24</sup> V. Bellani, E. Diez, R. Hey, L. Toni, L. Tarricone, G. B. Parravicini, F. Dominguez-Adame, and R. Gomez-Alcalá, Phys. Rev. Lett. **82**, 2159 (1999).

<sup>25</sup> F. M. Izrailev and N. M. Makarov, J. Phys.: Condens. Matter **38**, 10613 (2005).